Silicon (2023) 15:6257–6268
https://doi.org/10.1007/s12633-023-02488-2

RESEARCH

Surface Modification of Magnetite Using Silica Coating: Spectroscopic, Structural, Morphological Characterization and Interaction with Crystal Violet Dye

Amal Andolsi[1,2] · Islem Chaari[1] · Ahmed Hichem Hamzaoui[1]

Received: 3 March 2023 / Accepted: 23 April 2023 / Published online: 19 May 2023

Abstract
The essential goal of this work is to produce an eco-friendly and economically nano-adsorbent that may separate organic dye, especially, cationic dye, from polluted water prior to making use of this adsorbent in industrial field. This work suggests a way of fabricating magnetite and silica. The proposed approach concerned three steps: the preparation of magnetite (Fe_3O_4) nanoparticles by co-precipitation method, then of silica using sodium silicate prepared from silica sand, and finally a magnetite coating of silica Fe_3O_4/SiO_2. The nanocomposites were investigated by X-ray diffraction (XRD), Fourier transform infrared spectroscopy (FTIR) and transmission electron microscopy (TEM). The XRD characterization displayed that silica formed an amorphous phase and that magnetite shaped a spinel phase. To optimize the diverse experimental variables affecting the elimination performance of the CV, the effects of experimental parameters including solution pH, adsorbent dose, contact time, initial dye concentration and temperature were evaluated. Adsorption kinetic disclosed that pseudo-second-order is the best model ($R^2 > 0.99$, $q_e = 5.68$ mg g^{-1}). Adsorption isotherm represented that Langmuir is the best model with $Q_{max} = 200$ mg g^{-1}. The negative ΔH° and ΔG° values exhibited the exothermic and spontaneous nature of CV sorption on the nanoparticles, respectively.

Keywords Silica sand · $Fe_3O_4@SiO_2$ · Cristal violet dye · Characterization · Adsorption

1 Introduction

In current years, synthetic dyes have become one of the primary origin of water pollution. These pollutants are dangerous, carcinogenic and harmful to people, animals and plants [1]. Many decolorization techniques have been conducted for water treatment contaminated by the dye. These procedures are chemical, biological, and physical [2]. Physical methods including coagulation, adsorption, and oxidation have been proven for the purification of dye-containing effluent [3]. Adsorption is a successful physical remedy procedure for wastewater. It enables the removal of the organic pollutants in a cheap, direct, profitable, and straightforward manner, even if these pollutants exist in small quantities [4]. The high-quality technique for getting rid of the dye is adsorption because it is straightforward to use, inexpensive, very powerful and environmentally benign [5, 6]. Numerous materials have been. employed and examined, such as activated carbon, polymers, zeolite [7], clay [8] and nanomaterials [9] etc. Currently, magnetite nanoparticles have garnered strong attention for many contaminants, which include dyes due to their biocompatibility, high activity, excellent magnetic features, easy and the economic synthesis process [10]. Nowadays, they are several processes for the magnetite nanoparticles synthesis among them: co-precipitation [11], sol-gel [12], thermal decomposition [2], Hydrothermal [13], microwave irradiation, etc. Among them, co-precipitation is a crucial process, owing to it's a very simple, fast and inexpensive method and having a relatively low temperature in a short process [3–14]. After their fabrication, magnetite particles are unstable in the air; it is oxidized by oxygen of the air and

✉ Amal Andolsi
andolsiamal@yahoo.fr

Islem Chaari
chaari_islem@yahoo.fr

Ahmed Hichem Hamzaoui
mdmihi10@gmail.com

1 Useful Materials Valorization Laboratory, National Center of Research in Materials Sciences, Technopark Borj Cedria BP, 273 Hammam Lif, Tunisia

2 Faculty of Sciences of Tunisia, University of Tunisia El Manar, 2092 El Manar, Tunis, Tunisia

agglomerate easily [15] because of the dipolar interactions between them. Therefore, these nanoparticles demand functionalization and surface modification [16] by coating these particles with a layer of a material that is usually diamagnetic on the way to keep away from aggregation. The coating can be used with extra materials, including silica [17], polymers [18], carbon [19], clay [20], zeolite [21], etc. In this research, the magnetic particle (Fe_3O_4) changed into mixed with SiO_2 since it has a lot of benefits like the ability of its pure materials and the large capacity of cation exchange. Tunisia is a country with plentiful natural resources. Among them, silica sand. Silica has hydrophobic or hydrophilic properties based on its structure and morphology [22]. This material was employed in several factories and medical field owing to its biocompatibility, easy surface modification because of the abundant silanol groups, stability and its ability to absorb various substances such as water, oil, and radioactive material. In addition, coating procedure offers many advantages, such as simple method, low cost, availability of Tunisia sand, and credible time. To date, the majority of investigations have been synthesized silica coated by magnetite particles using Stőber process [23], which is an important method, as silica is formed in situ through the condensation of a sol–gel precursor as the tetraethyl orthosilicate (TEOS). Furthermore, few studies have been published regarding the fabrication of Fe_3O_4 @SiO_2 nanocomposites by natural material. For example, Taufiq et al. [24] synthesized silica-covered magnetite from natural sand.

The paper aims to synthesize nanomaterial magnetite by coprecipitation method and then coating with silica extracted from natural ressource to obtain Fe_3O_4@SiO_2 nanocomposites. The powders were studied using XRD, FTIR, SEM, TEM, and BET and applied as a magnetic adsorbent in the removal of crystal violet (CV) from aqueous solution. Several parameters such as pH, adsorbent dose, contact time, initial concentration of CV and temperature were investigated on the adsorption process. The kinetics, isotherms and thermodynamic parameters of adsorption were studied.

2 Experimental

2.1 Materials

The silica sand was sampled from the borj Hfayedh (Nabeul area, Northeast of Tunisia). Iron (III) chloride hexahydrate ($FeCl_36H_2O$), iron (II) sulfate heptahydrate ($FeSO_47H_2O$), sodium hydroxide, ammonium hydroxide were all purchased from Oxford lab Chem. (NH_3H_2O), ethanol (C_2H_5OH) and were purchased from Sigma Aldrich.

Cristal violet (CV) that also known C.I. 42,555 was purchased from Merck. The molecular weight for CV was 407.979 g mol^{-1} with a chemical formula of $C_{25}N_3H_{30}Cl$ and purity of 98%. For this purpose, 1000 mg L^{-1} of dye was inoculated into deionized water and then a serial dilution was prepared.

2.2 Synthesis of Fe_3O_4 and Fe_3O_4@SiO_2

Fe_3O_4 sample was synthesized via way of means of co-precipitation method. In this regard 0.8 g of $FeSO_4.7H_2O$ and 0.9 g of $FeCl_3.6H_2O$ were dissolved in distilled water (200 mL) and ethanol (40 mL) at 25 °C under the condition of vigorous stirring. After resting for 30 minutes, ammonium hydroxide (15 mL) was added dropwise into the solution as precipitating agent and solution color tends to change from brown to black. The acquired magnetite was amassed using a magnet, rinsed with distilled water to eliminate the surplus of ammonia and then dried in an oven at 60 °C for 8 h. Fe_3O_4@SiO_2 was prepared by the two step procedure (Fig. 1). Firstly, the used sand was washed and dried at 60 °C. Then it was completely mixed with 100 mL of sulfuric acid (2.5 M) for 48 h. The acid-treated sand was washed to eliminate the traces of the acid. After drying at 105 °C for 24 h, the obtained sample was crushed and sieved at 100 µm. Then, sand and sodium carbonate Na_2CO_3 (200 µm) were completely

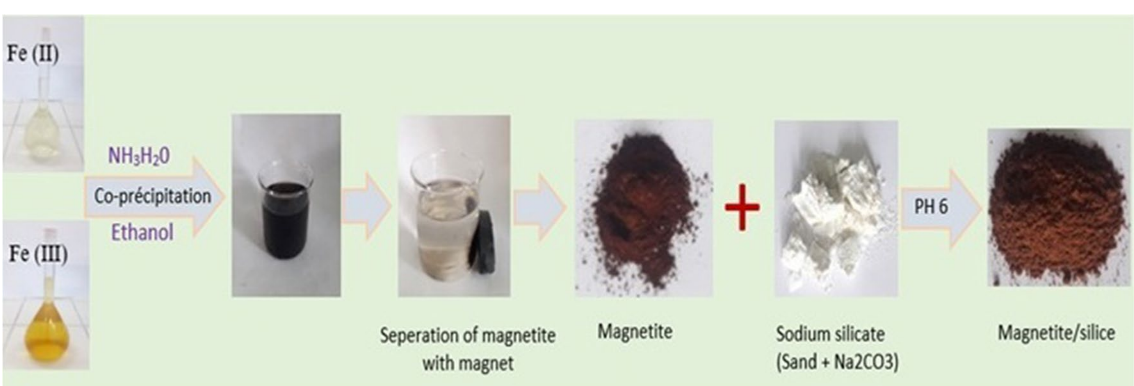

Fig. 1 Synthesis of Fe_3O_4 and Fe_3O_4@SiO_2

blended with a molar ratio $SiO_2/Na_2O = 1$ in high temperature (1060°C) to get the sodium silicate powder Na_2SiO_3. In the second step, 1.3 g of Na_2SiO_3 and 0.3 g of Fe_3O_4 have been dissolved in 100 mL of distilled water at 80 °C for 15 min and the pH 6 of the solution was adjusted using HCl (2 M). Then, the mixture was stirred at 80 °C for3h. The nanocomposites obtained (Fe_3O_4@ SiO_2) were separated through way of a magnet washed with water and dried at 60 °C for 8 h (Fig. 1).

2.3 Characterization

X-Ray diffraction analyses were performed using Bruker diffractometer model D8 advance under conditions of CuKα radiation (λ = 1.5406 Å). The system was operated at 40 kV and 30 mA. Diffraction patterns were recorded in the 2θ range of 10°–70°.

FTIR spectra were recorded in the region 4000 cm^{-1}-400 cm^{-1} (1 mg of the sample was prepared using KBr) with a perkin Elmer FTIR2000 infrared Fourier transform spectrometer.

The morphology of the materials was studied by scanning electron microscopy (SEM) microscope with a FEI Quanta 650.

The structural characteristics of the materials were studied by the means of TEM using the TECHNAI 20-Philips instrument (G20, 200 kV) equipped with an energy dispersive X-ray spectroscopy (EDX). The powders were ultrasonically dispersed in ethanol.

The nitrogen adsorption-desorption analysis at 77 K was determined by Micromeritics ASAP 2020 instrument. The Brunauer-Emmett-Teller (BET) and Barrett-Joyner (BJH) methods were used to determine the specific surface area (SSA) and the porosity.

The zeta potential measurement was determined by Malvern ZetaSizer Nano-SZ at different pH_S from 2 to 12. So, 1 mg of sample was suspended in 20 ml of 1 mM NaCl and shaked for 24 h. The point of zero charge (pH_{PCZ}) of the sample was found by plotting the zeta potential (mV) versus the pH.

2.4 Adsorption Test of CV on Fe_3O_4@SiO_2

Adsorption test was executed in a batch system with varying different parameters such as pH (2–10), adsorbent dose (0.001–0.1 g), contact time (5-180 min), initial concentration of the dye (10-500 mg L^{-1}) and temperature (25–55 °C). All experiments of adsorption were done on a 200 rpm stirrer until the system reached equilibrium. For this purpose, 0,05 g of Fe_3O_4@SiO_2 was added about 30 ml of CV (10 mg L^{-1}) at room temperature. The nanocomposites were separated by an external magnet and the residual CV concentration was measured by Agilent Cary6 UV-vis spectrophotometer of 590 nm. The CV adsorption rate (R) and the adsorption capacity (q_e) were calculated consistent with the subsequent equations (Eq. 1) (Eq. 2):

$$R(\%) = \frac{(C_0 - C_e)}{C_0} \times 100 \quad (1)$$

$$q_e = \frac{(C_0 - C_e)V}{M} \quad (2)$$

Where C_0 and C_e are the initial CV concentration and CV final concentration in mg L^{-1}, respectively. q_e is the CV uptake in mg g^{-1} adsorbent, Vis the volume of CV in mL and M is the quantity of nanocomposite in g.

3 Results and Discussion

3.1 Adsorbents Characterization

3.1.1 XRD Analysis

X-ray diffraction patterns of the Fe_3O_4 nanoparticles and Fe_3O_4@SiO_2 nanocomposites were presented in Fig. 2. For Fe_3O_4,diffraction peaks detected at 30.22°,35.65°,43.23°, 53.42°, 57.42, 62.79 and 71.41°corresponding to the (220), (311), (400), (422),(511), (440), (531) planes, respectively designated that Fe_3O_4 is cubic spinel structure [25, 26]. After silica coating on the magnetite surface, a broad peak observed for Fe_3O_4@SiO_2 at 2θ of 23°, was assigned to amorphous silica [27].The particle size may be determined by the following Debye–Scherrer equation (Eq. 3) [28]:

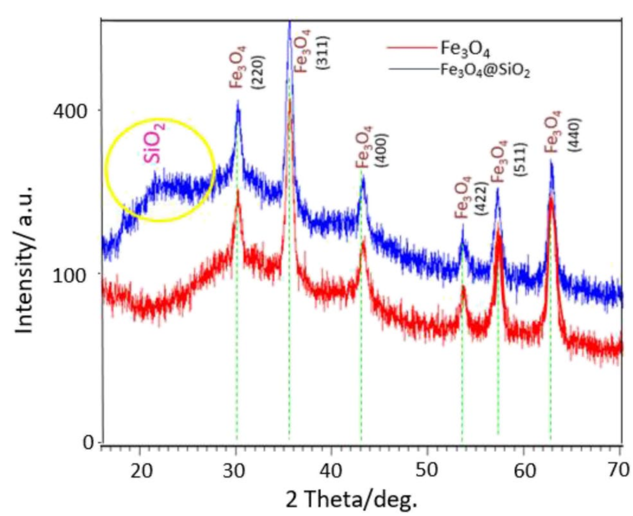

Fig. 2 XRD patterns of Fe_3O_4 and Fe_3O_4@SiO_2

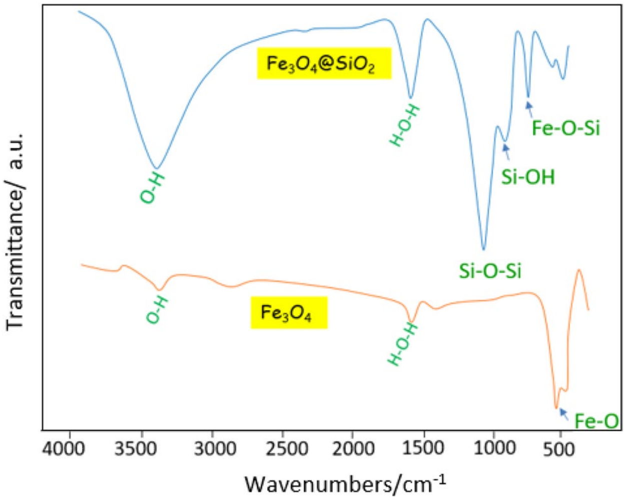

Fig. 3 FTIR spectra of Fe_3O_4 and $Fe_3O_4@SiO_2$

$$D = K\lambda/\beta\cos\theta \tag{3}$$

With D is the average diameter, K is Sherrer constant, λ is ray wavelength (0.15406 nm), β, the peak width of half-maximum, and θ, the Bragg peak angle. The Fe_3O_4 size was about 34.68 nm.

3.1.2 FTIR Analysis

The FTIR spectra of Fe_3O_4 and $Fe_3O_4@SiO_2$ were executed to confirm the existing of silica shell (Fig. 3).The band at 3464 cm^{-1} implied the existence of hydroxyl groups. Moreover, the band at 1641 cm^{-1} is assigned to H-O-H bending mode [29].The strong band at 584 cm^{-1} characterizing the Fe-O bonds confirm the spinel type structure of pure Fe_3O_4 nanoparticles [17]. In comparison with the curve of pure Fe_3O_4, the peaks at approximately 1091 cm^{-1}, 799 cm^{-1} and 460 cm^{-1} were ascribed to the symmetric and asymmetric stretching vibrations of Si-O-Si respectively. The peak at 960 cm^{-1} associated to Si-OH bond vibrations [29], which indicated the Fe_3O_4 was successful coated by SiO_2. This result has a good consent with the previous research [30].

3.1.3 SEM Analysis

SEM analysis was used to examine the morphology of the prepared samples, as seen in Fig. 4. Due to their small size and magnetism, the magnetic Fe_3O_4 nanoparticles in Fig. 4a exhibit an irregular crystalline shape, and surface morphology examination shows that they were agglomerated from several fine particles. When the Fe_3O_4 nanoparticules were covered with the SiO_2 layer, Fig. 4b demonstrates that the surface of the $Fe_3O_4@SiO_2$ nanocomposites was smoother and the agglomeration decreases than that of the Fe_3O_4 nanoparticles.

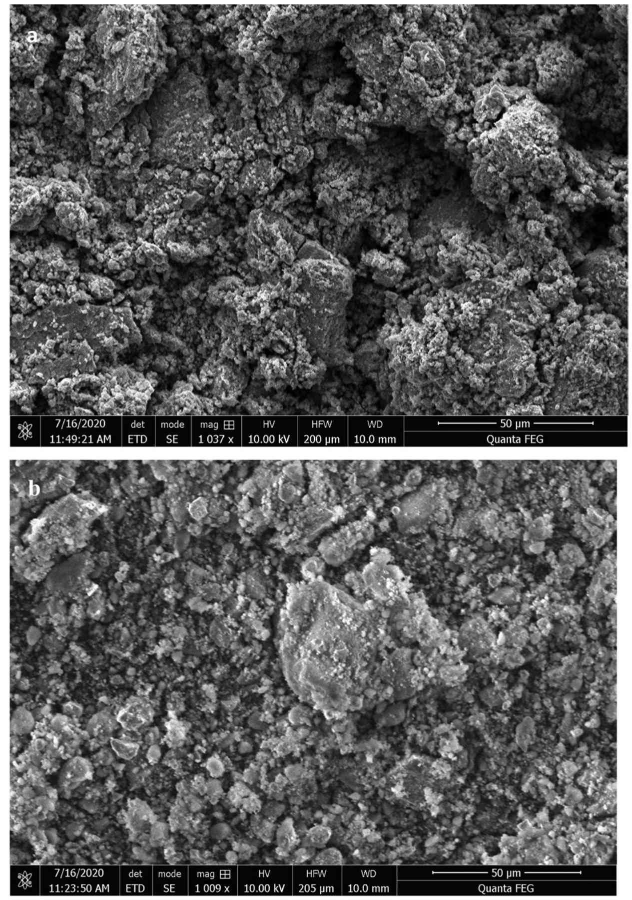

Fig. 4 SEM images of (**a**) Fe_3O_4 and (**b**) $Fe_3O_4@SiO_2$

3.1.4 TEM Analysis

TEM analysis, size distribution and EDX spectral profile Fe_3O_4 and the $Fe_3O_4@$ SiO_2 were observed in Fig. 5. TEM image of magnetite displays that particles are well dispersed with spherical forms (Fig. 5a) with ~ 34 nm diameter (Fig. 5c), which the same with size is obtained from XRD. Figure 5b reveals the TEM image of $Fe_3O_4@$ SiO_2. The size of this nanomaterial turned out to be approximately 36 nm for $Fe_3O_4@SiO_2$ (Fig. 5d). Moreover, (Fig. 5e-f) represents the EDX spectra of Fe_3O_4 and $Fe_3O_4@SiO_2$. As can be seen, the nanocomposites contain elements of silicium (Si), iron (Fe) and oxygen (O). Si band was determined in Fig. 5f after coating of magnetite with silica. In the elemental analysis, the basic composition of % Si, % Fe and O were defined.

3.1.5 Zeta Potential Analysis

The zeta potential evaluation of the $Fe_3O_4@SiO_2$ was assessed in the pH range of 2 to 12 and its result is displayed in Fig. 6. According to the results, the pHzpc

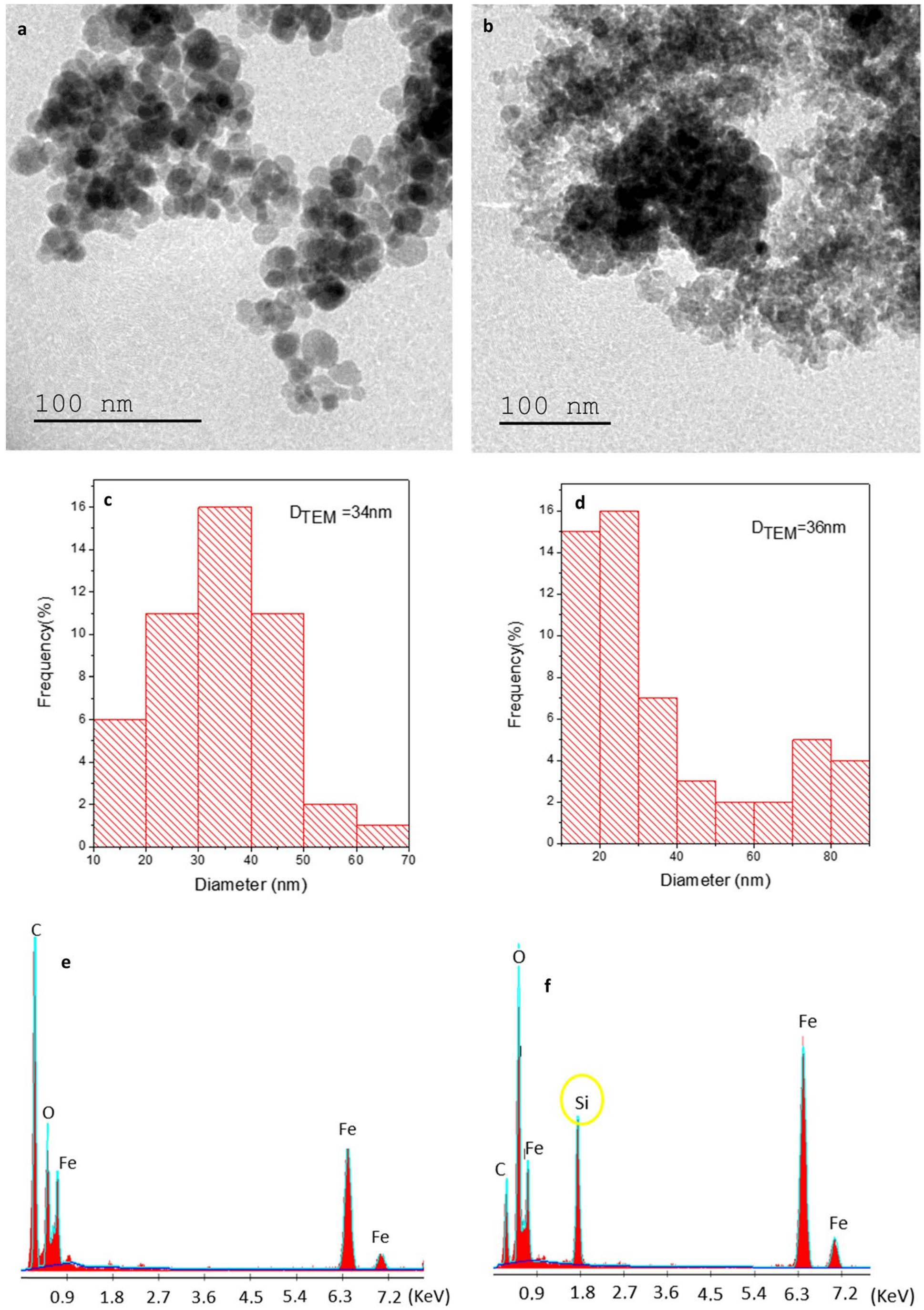

Fig. 5 TEM images of (**a**) Fe_3O_4 and (**b**) $Fe_3O_4@SiO_2$, and size distribution histogram of (**c**) Fe_3O_4 and (**d**) $Fe_3O_4@SiO_2$ obtained from the TEM micrograph, and EDX of (**e**) Fe_3O_4 and (**f**) $Fe_3O_4@SiO_2$

values had been acquired between 0 to −38.7 mV and the isoelectric point of the$Fe_3O_4@SiO_2$ was found to be approximately 2. This suggests that the $Fe_3O_4@SiO_2$ surface is negatively charged at pH above 2 that is favorable for the cationic CV adsorption. At very higher pH, there is electrostatic attraction between cationic CV and hydroxyl ions. Furthermore, at acidic pH, there is electrostatic repulsion between cationic CV and positively charged $Fe_3O_4@SiO_2$ surface along with the existence of hydrogen ions, which reduces the elimination performance at mentioned pH conditions.

3.1.6 Nitrogen Adsorption-Desorption Properties

The N_2 adsorption-desorption isotherms of Fe_3O_4 and $Fe_3O_4@SiO_2$ were discovered in Fig. 7a. The isotherms indicate type IV with an H3-type hysteresis loop, designate of the mesoporous structure of nanoparticles in keeping with the

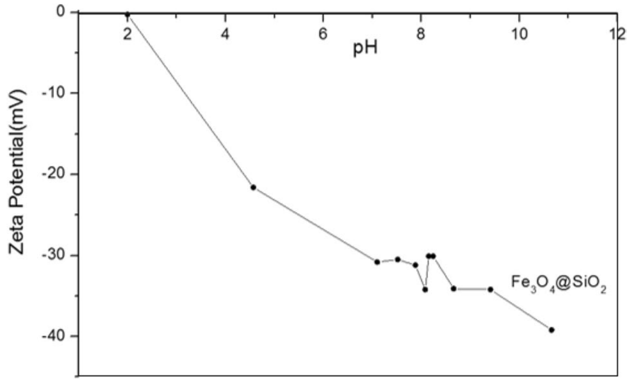

Fig. 6 Zeta potential analysis of $Fe_3O_4@SiO_2$

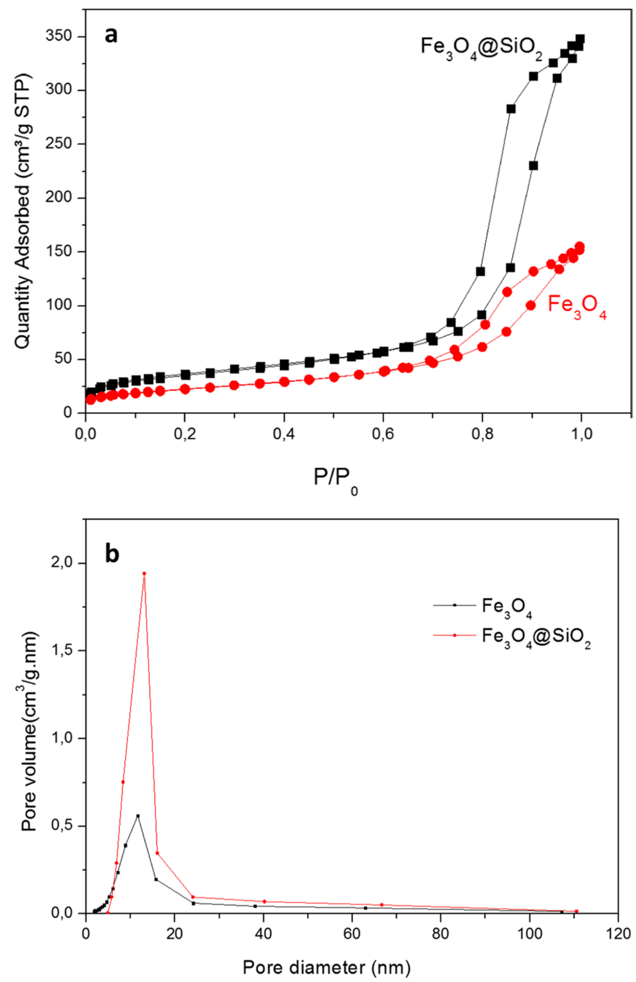

Fig. 7 (**a**) Nitrogen adsorption-desorption isotherms and (**b**) BJH pore size distribution curves of Fe_3O_4 and $Fe_3O_4@SiO_2$

IUPAC classification. The specific surface area of Fe_3O_4 and $Fe_3O_4@SiO_2$ were 81 and 133m^2/g, respectively. The increase in the specific surface area of $Fe_3O_4@SiO_2$ indicated that the existence of silica on the surface of Fe_3O_4, which favors the adsorption of dyes. The pore-size distribution measured by the BJH method of the prepared Fe_3O_4 and $Fe_3O_4@SiO_2$ as shown in Fig. 7b. The pore size distribution of Fe_3O_4 and $Fe_3O_4@SiO_2$ were 11.6 and 13 nm, respectively, designates a mesopore distribution. The pore size diameter of Fe_3O_4 and $Fe_3O_4@SiO_2$ were 9.6 and 11.3 nm, respectively, indicating the mesoporous structure. The pore volumes of Fe_3O_4 and $Fe_3O_4@SiO_2$ were 0.238 and 0.537 cm^3/g, respectively.

3.2 Elimination of CV under Varied Conditions

3.2.1 Effect of pH

The pH is the main parameter in the uptake of CV on the $Fe_3O_4@SiO_2$ nanocomposites. The results exhibited that the both adsorption capacity and CV adsorption rate improved by pH increase from 2 to 10 at a fixed initial dye concentration of 10 mg/L^{-1} and the adsorbent dose of 0.1 g and contact time of 180 min (Fig. 8). At acidic pH, the nanocomposites $Fe_3O_4@SiO_2$ and CV molecules were protonated and electrostatic repulsion interaction between protonated CV and positively charged $Fe_3O_4@SiO_2$ active sites lead to CV removal rate decrease [31]. The optimum pH value was fixed at pH 10. The same outcome was reported by Subhan et al. [32].

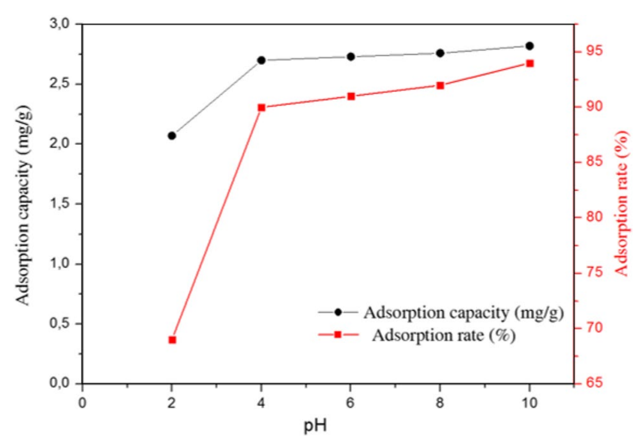

Fig. 8 Effect of pH on adsorption capacity and adsorption rate of CV on $Fe_3O_4@SiO_2$ (C_i = 10 mg L^{-1}, V = 30 ml, Time = 180 min, T = 298 K, Adsorbent dose = 0.1 g)

3.2.2 Effect of Adsorbent Dosage

The impact of adsorbent dose of adsorption capacity and CV adsorption rate was studied in the range of 0.005 g to 0.1 g for in initial concentration 10 mg L^{-1} and pH 10 and contact time 180 min. The results exhibited in Fig. 9. The adsorption capacity decreases from 195 to 2.82 mg g^{-1} with

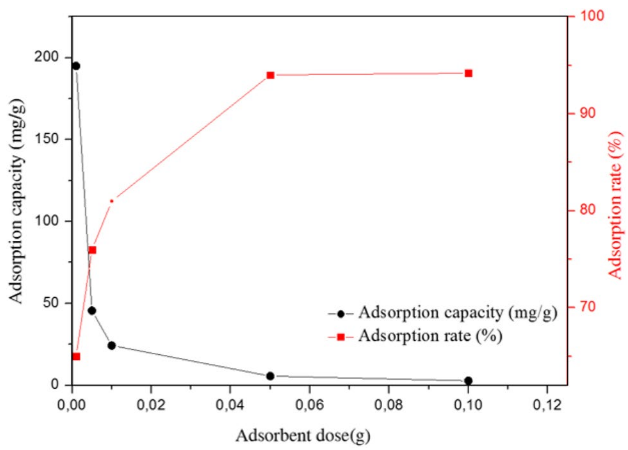

Fig. 9 Effect of adsorbent dose on adsorption capacity and adsorption rate of CV on $Fe_3O_4@SiO_2$ ($C_i = 10$ mg L^{-1}, V = 30 ml, Time = 180 min, T = 298 K, pH = 10)

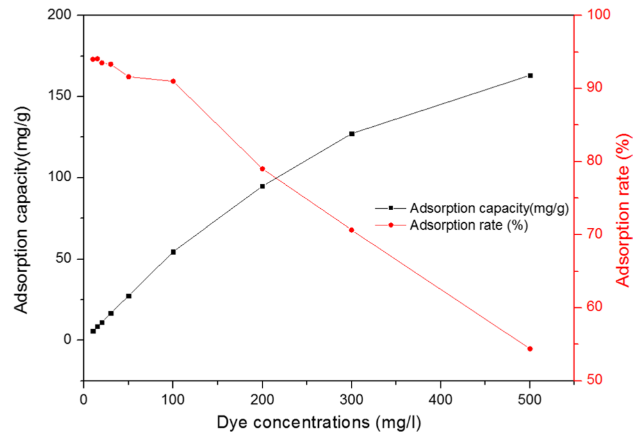

Fig. 11 Effect of initial dye concentration on adsorption capacity and adsorption rate of CV dye on $Fe_3O_4@SiO_2$ (adsorbent dose = 0.05 g, V = 30 ml, Time = 60 min, T = 298 K, pH = 10)

increasing adsorbent dose from 0.005 to 0.1 g that attributed to the availability of adsorption sites. However, the removal efficiency increases from 65 to 94% with increasing adsorbent dose as a consequence the higher number of active sites [9]. The nanosorbent dose was fixed at 0.05 g.

3.2.3 Influence of Contact Time

The time between pollutant and solid is a significant factor in wastewater purification; therefore, we also verified the decontamination period of the nanoadsorbent, as it is feasible to observe from Fig. 10. We discovered that the adsorption rate of CV increases rapidly over time. Based at the time study, 80.8% of CV dye was removed within 5 min. This trend in dye uptake is the result of the strong electrostatic interactions between CV and predominant silanol groups present on the outer surface of silica. Sorption equilibrium was attained in 60 min. At this time,the adsorbent surface becomes saturated. The test was pursued further for 120 minutes, but no significant increment was found in dye adsorption after 60 min shaking time. Therefore, remaining experiments were determined at 60 min.

3.2.4 Influence of Initial Dye Concentration

The influence of initial dye concentration of the adsorption of CV by $Fe_3O_4@SiO_2$ nanocomposites was carried at the range of 10 to 500 mg L^{-1} at fixed adsorbent dose 0.05 g, pH 10, contact time 60 min and room temperature. The adsorption capacity and CV adsorption rate was presented in Fig. 11. According to Fig. 11, the adsorption capacity was increased from

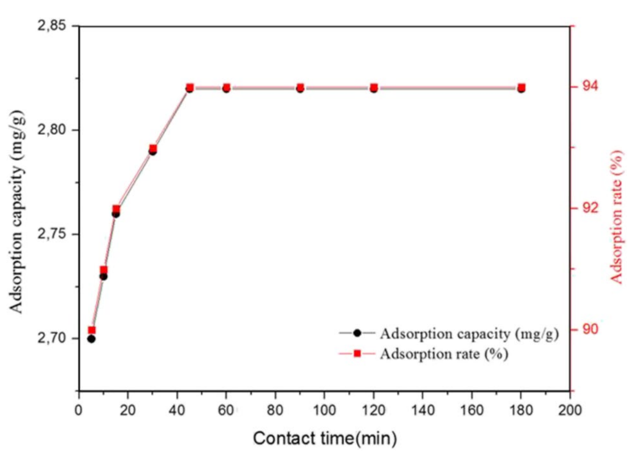

Fig. 10 Effect of contact time on adsorption capacity and adsorption rate of CV dye on $Fe_3O_4@SiO_2$ ($C_i = 10$ mg L^{-1}, V = 30 ml, T = 298 K, pH = 10, adsorbent dose =0.1 g)

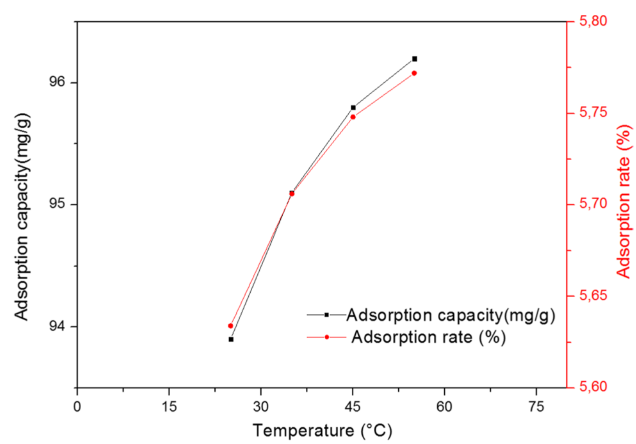

Fig. 12 Effect of temperature on adsorption capacity and adsorption rate of CV dye on $Fe_3O_4@SiO_2$ ($C_i = 10$ mg L^{-1}, adsorbent dose = 0.05 g, V = 30 ml, Time = 60 min, pH = 10)

Table 1 Estimated parameters of the kinetic models for the CV dye adsorption onto Fe_3O_4@SiO_2

Pseudo-first order			Pseudo-second order			
k_1 (min^{-1})	q (mg g^{-1})	R^2	q_{exp} (mg g^{-1})	k_2 (gmg^{-1} min^{-1})	q (mgg^{-1})	R^2
0.05	0.51	0.875	5.64	0.607	5.68	0.99

5.64 to 163.2 mg g^{-1} with increasing initial dye concentration 10–500 mg L^{-1}, respectively. The increase in the concentration of CV improves the interaction between the CV molecules and the surface of Fe_3O_4@SiO_2 nanocomposites. Although, The CV adsorption rate decreased from 94 to 54.4% with an increase in the CV concentration 10–500 mg l^{-1} because the active sites was saturated in the adsorbent surface [33].

3.2.5 Influence of Temperature

The effect of temperature of the adsorption of CV by the Fe_3O_4@SiO_2 nanocomposites was performed at several temperatures including 25, 35, 45, 55 °C for an initial concentration of 10 mg L^{-1} and pH of 10 and the adsorbent dose of 0.05 g and contact time of 60 min. The obtained results showed in Fig. 12. The adsorption capacity and CV adsorption rate increased from 5.63 to 5.77 mg g^{-1} and 93.9 to 96.2%, respectively when temperature increased from 25 to 55 °C. This indicates that the adsorption of CV by Fe_3O_4@SiO_2 nanocomposites was an endothermic process [34], which confirmed by the positive ΔH^o parameter on thermodynamic adsorption. The increase in the temperature reaction induces to changes in the size of the pores, the kinetic energy of CV molecules and the increase in diffusion rates [35].

3.2.6 Adsorption Kinetics

To explore the rate of CV adsorption by the nonabsorbent, the pseudo-first-order (Eq. 4) [36] and the pseudo-second-order (Eq. 5) [37] models were adopted to correlate the time-dependent sorption data.

$$\ln\left(q_{eq} - q_t\right) = \ln q_{eq} - \frac{k_1}{2.303}t \quad (4)$$

$$\frac{t}{q_t} = \frac{1}{k_2 {q_{eq}}^2} + \frac{1}{q_{eq}}t \quad (5)$$

With,

q_{eq}: Amount of CV adsorbed at equilibrium (mg/g); q_t: Amount of CV adsorbed on Fe_3O_4@SiO_2 (mg g^{-1}) at the instant t; k_1 (min^{-1}) and k_2 (g mg^{-1} min^{-1}): Pseudo-first and Pseudo-second rate constants.

The parameters of these kinetic models have been summarized in Table 1. The highest correlation (R^2), and good conformity between the $q_{eq,exp}$ and $q_{eq,cal}$ values exhibited that the uptake of CV onto Fe_3O_4@SiO_2 could be well modeled with the pseudo-second-order, which is similar to the outcomes found by some other researchers for dye adsorption.

3.2.7 Adsorption Isotherms

The experimental data for CV on the Fe_3O_4@SiO_2 were fitted by the Langmuir and Freundlich models. Such models designate the sorption mechanism between CV and nanocomposites. The two models are expressed by (Eq. 6) and (Eq. 7).

Langmuir model [38]:

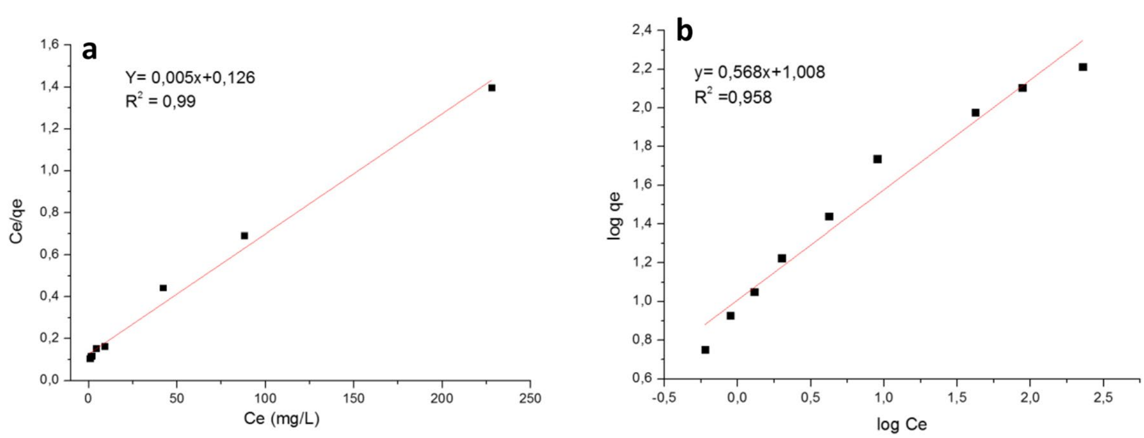

Fig. 13 Langumir isotherms (**a**) and Freundlich isotherm (**b**) for adsorption of CV on Fe_3O_4@SiO_2

Table 2 Isotherms parameters for CV adsorption onto Fe_3O_4@ SiO_2

Langmuir					Freundlich		
K_L	R^2	R_L	Q_m (mg g^{-1})	.	K_F	n	R^2
0.0045	0.98	0.818	200		2.76	1.736	0.958

$$q_{eq} = \frac{Q_m K_L C_{eq}}{1 + K_L C_{eq}} \quad (6)$$

Where C_{eq} (mg l^{-1}) is the equilibrium concentration of CV, q_{eq} (mg g^{-1}) is the equilibrium adsorption ability and Q_m is a quantity of CV fixed per gram of nanosorbent (mg g^{-1}). In addition, K_L is the empirical constant.

Freundlich model [39]:

$$q_{eq} = K_F C_{eq}{}^{1/n} \quad (7)$$

With, K_F (mg g^{-1})/(Lmg^{-1})^n is adsorption capacity.

The Langmuir model correlated higher to the investigated procedure in assessment with that of the Freundlich model (Fig. 13) utilizing the experimental outcomes for the uptake equilibrium of CV by nanocomposites (Table 2), therefore, it may be deduced that the adsorption sites are homogeneous. Likewise, Q_m for nanocomposites is 200 mg g^{-1}. The adsorption capacity of Fe_3O_4@SiO_2 has been compared with different nanosorbents (Table 3). As can be observed, the Fe_3O_4@SiO_2 Q_m value is more than this other adsorbents.

3.2.8 Thermodynamic Study

To understand the thermodynamic performances of CV adsorption onto Fe_3O_4@SiO_2, thermodynamic functions were evaluated. Thermodynamic parameters, i.e., the change in the Gibbs free energy (ΔG°, kJ mol^{-1}), the change in enthalpy (ΔH^o, kJ mol^{-1}), and the change in entropy (ΔS°, J mol^{-1} K^{-1}), are used to evaluate the thermodynamic feasibility and the nature of the process. The ΔH° (Eq. 8), ΔS° (Eq. 9), and ΔG° (Eq. 10) parameters were determined [44] and are listed in Table 4.

$$\Delta G^0 = -RTlnk_d \quad (8)$$

$$k_d = \frac{q_{eq}}{C_{eq}} \quad (9)$$

$$\ln k_d = \frac{\Delta S^0}{R} - \frac{\Delta H^0}{RT} \quad (10)$$

Table 4 exhibits the calculated data. The negative values of ΔG° verify the feasibility and spontaneity of the adsorption of CV dye on Fe_3O_4@SiO_2. Additionally, the value of ΔG° changed from −5.46 to −7.46 kJ mol^{-1}, whereas the temperature increased from 298 to 328 K, this suggesting that adsorption is highly spontaneous at higher temperatures.

The positive value of ΔH°, confirm the endothermic nature of the sorption process and the possibility of physical adsorption [45]. The positive values of ΔH° suggest the enhancement in randomness at the Fe_3O_4@SiO_2/liquid interface with some structural modifications in the solute and material as well as the good affinity of Fe_3O_4@SiO_2 for the CV [46].

3.2.9 Adsorption Mechanism

The Fe_3O_4@SiO_2 surface contains active sites; these sites gave a platform for CV to adsorb on it Fig. 14 depicted a schematic sketch for the sorption mechanism of CV dye molecule onto Fe_3O_4@SiO_2 nanoadsorbent. Silica was first used to coat Fe_3O_4nanoparticles and then to synthesize Fe_3O_4@SiO_2nanocomposites to ameliorate the surface area and consequently the number of adsorption sites. As mentioned early, after caoating, the SSA increases from 81 to 133 m^2g^{-1}. Therefore, the nanocomposites Fe_3O_4@SiO_2, which surface consists of silicium, carbon, oxygen, and iron was finally used as a nanoadsorbent for decolorization of textile waste water. In fact, pH affected the adsorption

Table 3 Comparison of maximum monolayer adsorption capacities of CV onto Fe_3O_4@SiO_2

Adsorbents	Q_m (mg g^{-1})	References
Fe_3O_4@ clinoptilolite	44.052	[40]
Magnetite Alginate	37.5	[41]
Fe_3O_4/ActivatedCarbon	35.31	[42]
Fe_3O_4@chitosan	183.2	[43]
$Fe_3O_4SiO_2$	200	This work

Table 4 Thermodynamic parameters for adsorption of CV onto Fe_3O_4@SiO_2

Temperature (K)	ΔG° (KJ mol^{-1})	ΔH° (J mol^{-1})	ΔS° (J mol^{-1} K^{-1})
298	−5.46		
308	−6.17	188.81	25.95
318	−6.91		
328	−7.42		

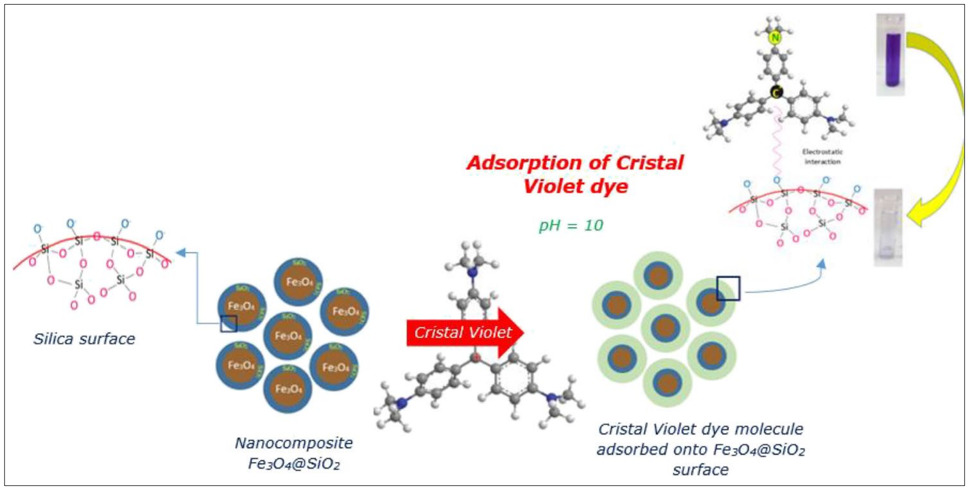

Fig. 14 Schematic sketch for the sorption mechanism of CV dye molecule onto Fe_3O_4@SiO_2nano-adsorbent

behavior and mechanism. At pH = 10, the surface functional groups of Fe_3O_4@SiO_2 were deprotonated and made it negatively charged. This negative charge resulted in electrostatic interaction with positively charged groups of CV. While decreasing the pH, the surface charge density of Fe_3O_4@SiO_2 increased due to protonation, and electrostatic repulsion between positive CV and Fe_3O_4@SiO_2 surface lowered the percentage adsorption.

4 Conclusions

Fe_3O_4@SiO_2 core–shell nanocomposites were synthesized by siliceous sand using co-precipitation method. Fourier transforms infrared spectra and X-ray diffraction revealed that Fe_3O_4 was successfully coated by silica. According to TEM results, the Fe_3O_4 was spherical, regular in shape, and the SiO_2 coating layer was uniform. The size of Fe_3O_4 and Fe_3O_4@SiO_2 were about 34 and 36 nm, respectively. The BET method indicated that the coating of the surface of magnetite by silica increases the surface area of Fe_3O_4@SiO_2 compared with Fe_3O_4. Moreover, this work primarily aimed at determining the optimal variant of the process to maximize the adsorption rate (R) and the adsorption capacity (q_e). The findings displayed that the optimum conditions for the solution pH, contact time, sorbent amount and initial dye concentration were 10.0, 60 min, 0.05 g, 10 mg L^{-1} respectively, were given maximum R of 94% and an at most capacity Q_{max} of 200 mg g^{-1}. Thermodynamic parameters designated that CV adsorption on Fe_3O_4@SiO_2 was endothermic. In this work, the silica coated magnetite as a low-cost material is highly efficient and well suited for the elimination of dyes and in particular CV.

Acknowledgments The authors are thankful to Mr. Mounir Hajji from Centre National de Recherches en Sciences des Materiaux for his help with synthesis of sodium silicate.

Authors' Contributions Andolsi Amal, Chaari Islem, Hamzaoui Ahmad Hichem: prepared the research, and interpret household survey data and wrote research report draft. Hamzaoui Ahmad Hichem, Chaari Islem: conceptualization and methodology. All authors edit and revised the manuscript and approved it to send to the journal.

Funding The study was fnancially supported by National Center of Research in Material Sciences.

Data Availability The authors declare that the data supporting the findings of this study are available within the article and its supplementary information are available by request.

Declarations

Competing Interests The authors have non relevant financial or non-financial to disclose.

Ethical Approval Not Applicable.

Consent for Publications All the authors of the manuscript mutually agree on submission and publication in the journal.

Consent to Participate All Authors contributed to the work and revised the manuscript.

References

1. Zangeneh H, Zinatizadeh AAL, Habib M, Akia M, Hasnain Isa M (2015) Photo-catalytic oxidation of organic dyes and pollutants in waste water using different modified titanium dioxides: a comparatives review. J Ing Eng Chem 26:1–36. https://doi.org/10.1016/j.jiec.2014.10.043
2. Roca AG, Morales MP, O'Grady K (2006) Structural and magnetic properties of uniform magnetite nanoparticles prepared by high temperature decomposition of organic precursors. Nanotechnol 17:2783–2788. https://doi.org/10.1088/0957-4484/17/11/010
3. Maity D, Choo SG, Yi J, Ding J, MinXue J (2009) Synthesis of magnetite nanoparticles via a solvent-free thermal decomposition route. J MagnMagn Mater 321:1256–1259. https://doi.org/10.1016/j.jmmm.2008.11.013

4. Salem ANM, Ahmed MA, El-Shahat MF (2016) Selective adsorption of amaranth dye onFe_3O_4/MgO nanoparticles. J Mol Liq 219:780–788. https://doi.org/10.1016/j.molliq.2016.03.084
5. Han X, Chu L, Liu S, Chen T, Ding C, Yan J, Cui L, Quan G (2015) Removal of methylene blue from aqueous solution using porous biochar obtained by KOH activation of peanut shell biochar. Bio Resour 10:2836–2849. https://doi.org/10.15376/biores.10.2.2836-2849
6. Joshiba GJ, Kumar PS, Christopher FC, Pooja G, Kumar VV (2020) Fabrication of novel amine-functionalized magnetic silica nanoparticles for toxic metals: kinetic and isotherm modelling. Environ Sci Pollut Res Int 27:27202–27210. https://doi.org/10.1007/s11356-019-05186-y
7. Ismail AM, Menazea AA, Ali H (2021) Selective adsorption of cationic azo dyes onto zeolite nanorod-based membranes prepared via laser ablation. J Mater Sci Electron 32:19352–19367. https://doi.org/10.1007/s10854-021-06453-w
8. Chaari I, Medhioub M, Jamoussi F, Hamzaoui AH (2020) Acid-treated clay materials (southwestern Tunisia) for removing sodium leuco-vat dye: characterization, adsorption study and activation mechanism. J Mol Struct 1223:128944. https://doi.org/10.1016/j.molstruc.2020.128944
9. Ghorbani F, Kamari S (2019) Core–shell magnetic nanocomposite of Fe_3O_4@SiO_2@NH_2 as an efficient and highly recyclable adsorbent of methyl red dye from aqueous environments. Environ Technol Innov 14:100333
10. Zhang Z, Kong J (2011) Novel magneticfe_3O_4@C nanoparticles as adsorbents for removal of organic dyes from aqueous solution. J Hazard Mater 193:325–329. https://doi.org/10.1016/j.jhazmat.2011.07.033
11. Hariani PL, Faizal M, Marsi R, Setiabudidaya D (2013) Synthesis and properties of Fe_3O_4 nanoparticles by co-precipitation method to removal Procion dye. Int J Environ Sci Dev 4. https://doi.org/10.7763/IJESD.2013.V4.366
12. Takai ZI, Mustafa MK, Asman S, Khairunnadim AS (2019) Preparation and characterization of magnetite (Fe_3O_4) nanoparticles by sol-gel method. In J Nanoelectron Mater 12:37–46
13. Ge S, Shi X, Sun K, Li C, Uher C, Baker JR, Banaszak Holl MM, Orr BG (2009) Facile hydrothermal synthesis of Iron oxide nanoparticles with tunable magnetic properties. J Phys Chem C Nanomater Interface 113:13593–13599. https://doi.org/10.1021/jp902953t
14. Morales F, Márquez G, Sagredo V, Torres TE, Denardin JC (2019) Structural and magnetic properties of silica-coated magnetite nanoaggregates. Phys B Condens Matter 572:214–219. https://doi.org/10.1016/j.physb.2019.08.007
15. Huang J, Liu W, Liang Y, Li L, Duan L, Chen J, Zhu F, Lai Y, Zhu W, You W, Jia Z, Xiong J, Wang D (2018) Preparation and biocompatibility of diphasic magnetic nanocomposite scaffold. Mater Sci Eng C 87:70–77. https://doi.org/10.1016/j.msec.2018.02.003
16. Lu AH, Salabas EL, Schüth F (2007) Magnetic nanoparticles: synthesis, protection, functionalization, and application. Angew ChemInt EdEng 46:1222–1244. https://doi.org/10.1002/anie.200602866
17. Zhang L, Shao HP, Zheng H, Lin T, Guo ZM (2016) Synthesis and characterization of Fe_3O_4@SiO_2 magnetic composite nanoparticles by a one-pot process. Int J Miner Metall Matter 23:1112–1118. https://doi.org/10.1007/s12613-016-1329-6
18. Lee HJ, Lu Q, Lee JY, Jin Choi H (2019) Polymer-Magnetic-CompositeParticles of Fe_3O_4/poly (*o*-anisidine) and their suspension characteristics under applied magnetic fields. Polym 11:219. https://doi.org/10.3390/polym11020219
19. Kakvandi B, Jonidi A, Kalantary RR (2013) Synthesis and Propertiesof Fe3O4-activated carbon magnetic nanoparticles for Remova lof aniline from aqueous solution: equilibrium, kinetic and thermodynamic studies. Irn J Environ Health Sci Eng 10:19
20. Shah KH, Ali S, Shah F (2018) Magnetic oxide nanoparticles (Fe_3O_4) impregnated bentonite clay as a potential adsorbent for Cr (III) adsorption. Mater Res Express 5:096102. https://doi.org/10.1088/2053-1591/aad50e
21. Ahmad ARD, Imam SS, Oh WD (2020) Fe_3O_4-zeolite hybrid material as hetero-Fenton catalyst for enhanced degradation of aqueous Ofloxacin solution. Catalysts 10:1241. https://doi.org/10.3390/catal10111241
22. Zhao Y, Li J, Zhao L, Zhang S, Huang Y, Wu X, Wang X (2014) Synthesis of amidoximme-functionalized Fe3O4@SiO2 core–shell magnetic for highly efficient sorptionof U(VI). Chem Eng J 235:275–283. https://doi.org/10.1016/j.cej.2013.09.034
23. Furlan PY, Furlan AY, Kisslinger K (2019) Water as the solvent in the Stober process for forming ultrafine silica shells on magnetite nanoparticles. ACS Sustain Chem Eng 7:15578–15584. https://doi.org/10.1021/acssuschemeng.9b03554
24. Taufiq A, Nikmah A, Hidayat A, Sunaryono S, Mufti N, Susanto N (2020) Synthesis of magnetite/silica from sand to create a delivery vehicle. Heliyon 6:e03784. https://doi.org/10.1016/j.heliyon.2020.e03784
25. Huang C, Hu B (2008) Silica-coated magnetic nanoparticles modified with γ- mercaptopropyltrimethoxysilane for fast and selective solid phase extraction of trace amounts of Cd,Cu,Hg, and Pb in environmental and biological samples prior to their determination by inductively coupled plasma massspectrometry. Spectrochim Acta B At Spectrosc 63:437–444. https://doi.org/10.1016/j.sab.2007.12.010
26. Kakavandi B, Jahangiri-rad M, Rafiee M, Esfahani AR, Babaei AA (2016) Develpement of response surface methodology for optimization of pheneol and p-chlorophenol adsorption on magnetic recoverable carbon. Microporous Mesoporous Mater 231:192–206. https://doi.org/10.1016/j.micromeso.2016.05.033
27. Grass RN, Athanassiou EK, Stark WJ (2007) Covalently functionalized cobalt nanoparticles as a platform for magnetic separations in organic synthesis. Angew Chem Int Ed 46:4909–4912. https://doi.org/10.1002/anie.200700613
28. Ding BJ, Chen WM, Fan LW, Zheng YH, Lv D, Lu ZX (2014) Preparation and characterization of Fe_3O_4@SiO_2 magnetic catalyst support. Inorg Chem Ind 46:62
29. Kazemzadeh H, Ataie A, Rashchi F (2012) In situ synthesis of silica-coated magnetite nanoparticles by reverse Coprecipitation method. J Supercond Nov Magn 25:2803–2808. https://doi.org/10.1007/s10948-011-1270-x
30. Yoshino H, Kamiya K, Nasu HIR (1990) Study on the structural evolution of sol-gel derived SiO_2gels in the early stage of conversion to glasses. J Non-Cryst Solids 126:68–78. https://doi.org/10.1016/0022-3093(90)91024-L
31. Hameed B, El-kaiary M (2008) Remval of basic dye from aqueous medium using a novel agricultural waste material. Pumpkin seed hullJ Hasard Mater 155:601–609. https://doi.org/10.1016/j.jhazmat.2007.11.102
32. Subhan F, Aslam S, Yan Z, Khan M, Etim UI, Naeem M (2019) Effective adsorptive performance of Fe_3O_4@SiO_2 core shell spheres for methylene blue: kinetics,isotherm and mechanism. J Porous Mater 26:1465–1474. https://doi.org/10.1007/s10934-019-00744-8
33. Deng H, Lu J, Li G, Zang G, Wang X (2011) Adsorption of methylene blue on adsorbent materials produced from cotton stalk. Chem Eng J 172:326–334. https://doi.org/10.1016/j.cej.2011.06.013
34. Abu Auwal M, Hossen J, Rakib-uz-Zaman M (2018) Removal of phenol from aqueous solution using tamarind seed powder as adsorbent. J Env Sci Toxi Fod Tech 12:41–48. https://doi.org/10.9790/2402-1203014148

35. Arnata W, Suprihatin FF, Richana N, Candra Sunarti T (2019) Adsorption of anionic Congo red dye by using cellulose from sago frond. Pollut Res 38:557–567
36. Lagergren S (1898) About the theory of so-calledadsorption of substances Kungliga Svenska Vetenskaps akademiens. Handlingar Band 24:1–39
37. Ho YS, McKay G (1998) Sorption of dye from aqueous solution by peat. Chem Eng J 70:115–124. https://doi.org/10.1016/S0923-0467(98)00076-1
38. Langmuir I (1918) The constitution and fundamental properties of solids and liquids. J Am Chem Soc 40:1361. https://doi.org/10.1016/S0016-0032(17)90938-X
39. Freundlich HMF (1906) Uber die adsorption ilosungen. Z Phys Chem 57:385–470. https://doi.org/10.1515/zpch-1907-5723
40. Noori M, Tahmasebpoor M, Nami SH (2022) Adsorption removal of crystal violet in single and binary systems onto low-costiron oxide nanoparticles coated clinoptilolite powders/granules. https://doi.org/10.21203/rs.3.rs-1727993/v1
41. Elwakeel KZ, El-Bindary AA, El-Sonbati AZ, Hawas AR (2017) Magnetic alginate beads with high basic dye removal potential and excellent regeneration ability. Can J Chem 95:807–815. https://doi.org/10.1139/cjc-2016-0641
42. Foroutan R, Peighambardoust SJ, Peighambardoust SH, Pateiro M, Lorenzo JM (2021) Adsorption of CrystalViolet dye using activated carbon of Lemn wood and activated carbon/Fe3O4 magnetic nanocomposite from AqueousSolutions: a kinetic equilibrium and thermodynamic study. Mole 26:2241. https://doi.org/10.3390/molecules26082241
43. Du Y, Pei M, He Y, Yu F, Guo W, Wang L (2014) Preparation, characterization and application of magnetic Fe_3O_4-CS for the adsorption of Orange I from aqueous solutions. PLoS One 9:e108647. https://doi.org/10.1371/journal.pone.0108647
44. Mohebali S, Bastani D, Shayesteh H (2019) Equilibrium kinetic and thermodynamic studies of a low-cost biosorbent for the removal of Congo red dye: acid and CTAB-acid modified celery *Apium graveolens*. J Mol Struct 1176:181–193. https://doi.org/10.1016/j.molstruc.2018.08.068
45. Scheufele FB, Staudt J, Ueda MH, Caroline R, Steffen V, Borba CE, M'odenes AN, Kroumov AD (2020) Biosorption of direct black dye by cassavaroot husks: Kinetics,equilibrium, thermodynamics and mechanism assessment. J Environ Chem Eng 8:103533. https://doi.org/10.1016/j.jece.2019.103533
46. Alqadami AA, Naushad M, Abdalla MA, Khan MR, Alothman ZA (2016) Adsorptive removal of toxic dye using Fe_3O_4–TSC nanocomposite: equilibrium kinetic and thermodynamic studies. J Chem Eng Data 61:3806–3813. https://doi.org/10.1021/acs.jced.6b00446